Developing fracture-based fragility curves for steel components in corrosive environments

Mohammad Ali Mahdavipour[1], Dmitry Vysochinskiy[2]

[1] Ph.D. Research Fellow, Department of Engineering Sciences, University of Agder, Jon Lilletuns vei 9, 4879, Grimstad, Norway, Email: ali.mahdavipour@uia.no

[2]Associate Professor, Department of Engineering Sciences, University of Agder, Jon Lilletuns vei 9, 4879, Grimstad, Norway, Email: dmitry.vysochinskiy@uia.no

Abstract

Under excessive plastic deformations, pitting corrosion accelerates ductile fracture initiation in steel components. Because of the stochastic and time-dependent nature of corrosion in steel material, the integrity of the steel components must be evaluated through a rational procedure in which corrosion uncertainties are considered to estimate the probability of failure for future events. Previous studies developed fragility curves to predict the capacity of global structures under uniform corrosion. However, for steel structures subjected to pitting corrosion, the local effect of corrosion is substantial and is also challenging to implement in the global model of structures. In this study, the concept of fracture-based fragility curves was developed at the component level by micromechanical modeling of different random pitting morphologies at a given intensity level of pitting corrosion. For this purpose, a unique meshing technique was employed to implement random pitting morphologies in numerical models. A demonstration study on a single-sided corroded plate revealed that random morphologies at an identical corrosion intensity level led to a notable dispersion in the failure elongations. The proposed fragility curves could address this effect on the probability of failure of the specimen. Therefore, decision-makers can reliably utilize such curves in a comprehensive risk-based corrosion management framework to evaluate the risk of failures and determine proper treatment strategies.

KEYWORDS

Fragility curve; pitting corrosion; steel marine structure; ductile fracture; excessive plastic deformation; probability of failure

1. Introduction

Many of the worlds' structures like bridges, jetties, offshore facilities are subjected to aggressive environments. For these structures, structural integrity and safety must be demonstrated concerning the interaction of possible loading scenarios and the corrosion deterioration (DNV GL 2015a). Because of the stochastic and time-dependent nature of corrosion in steel material, this interactional effect must be studied through a comprehensive risk-based corrosion management framework (DNV GL 2015a).

In a risk-based corrosion management procedure, the risk is identified based on the potential threats and consequences of the current and future corrosion to the structural integrity (DNV GL 2015a). In this procedure, the analysis of the likelihood of failures and their consequences to the whole system plays a central role in performing a quantitative risk assessment (DNV GL 2015a). Based on such evaluated likelihoods, the risk managers can choose proper treatment techniques to upgrade existing structures to fulfill principal criteria, e.g., health and safety, economy, environment, etc. (DNV GL 2015a). Furthermore, the risk evaluation of failure in the design phase of new structures subjected to corrosion is also essential to facilitate an optimal selection of corrosion prevention, inspection, and monitoring methods based on the structure's performance for future events.

In order to perform corrosion risk evaluations, fragility curves are viable statistical tools because they quantify the failure of the aged structures in terms of probability. Fragility curves have been widely employed for the assessment of various structures subjected to corrosion. Ghosh and Padgett (2010); Guo and Zhang (2019), and Yang et al. (2021) developed fragility curves for different aged reinforced concrete structures under seismic loads. In these studies, the corrosion was considered as a uniform reduction in the sectional area of the rebars. Jahanitabar and Bargi (2018); (Yang et al. 2019), and (Yeter et al. 2020) conducted similar studies to develop seismic fragility curves for steel structures affected by uniform corrosion.

All the above-mentioned studies used the concept of fragility curves to predict the capacity of an aged structure at the global level. This approach is mainly applicable to structures with uniform corrosion, that the effect of corrosion deterioration can be implemented in macro models or simplified shell models by reducing the section of the corroded members. However, for steel structures subjected to pitting corrosion, the local effect of corrosion is substantial. Modeling this local effect in the global structures is challenging due to numerical models and computational

resources limitations. This issue will be more challenging when structures are under extreme loads that cause excessive plastic deformations. In such a scenario, corrosion pits act as local concentrators that magnify the local plastic strain and stress triaxiality (Cerit 2013; Ji et al. 2015; Pidaparti and Patel 2008; Turnbull et al. 2010). This magnification can accelerate ductile fracture initiation in steel components (Bao and Wierzbicki 2004; Hancock and Mackenzie 1976; Johnson and Cook 1985; McClintock 1968; Rice and Tracey 1969) and can reduce their ductility significantly. In addition, previous studies (Ahmmad and Sumi 2010; Songbo et al. 2021; Wang et al. 2018a; Wang et al. 2017; Xu et al. 2016; Zhao et al. 2020) indicated that a three-dimensional representation of the pit geometry associated with a micromechanical fracture criterion is required to accurately capture the local effects of pitting on the ductile fracture of a component. In such numerical models, a fine discretization of the corrosion spatial geometry must be utilized to predict the local responses properly (Ahmmad and Sumi 2010; Songbo et al. 2021; Wang et al. 2018a; Wang et al. 2017). As a result, fragility curves obtained based on the macro modeling approach or shell modeling with an equivalent thickness cannot properly describe the effect of the random pitting in the prediction of failure of the structures (Wang et al. 2018b).

The limitations mentioned above motivated the authors to introduce fracture-based fragility curves at the component level of corroded steel structures subjected to marine environments. For a given intensity level of pitting corrosion, the fragility curves were produced by micromechanical modeling of different random pitting morphologies. In this connection, pitting morphologies were generated randomly based on the probability distributions of pit characteristics and were implemented based on a proposed meshing technique. The developed fragility curves are capable to reliably assess the integrity of steel components under large plastic deformations where ductile fracture is a probable failure mode. As a result, the proposed approach can be extended to real scenarios like a ship collision, an unexpected element removal, or a dropped heavy object in which excessive plastic deformations are expected. Under those circumstances, each component contributes to the reliability or failure of the system (Lemaire 2013). Therefore, the component fragility curves enable engineers to characterize the most critical failure scenario based on combinations of component failures (Lemaire 2013).

It is worth mentioning that proposed fragility curves are applicable for both general and pitting corrosion or a combination of them; however, in this study, only the

pitting corrosion was considered that is believed to be the main source of the corrosion uncertainties.

2. Methodology

Fig. 1 illustrates an overview of the risk-based corrosion management procedure consists of three main modules. These modules form a life cycle in which a continuous assessment is done to keep the risk of corrosion updated and accordingly to determine the expected life of the facilities and revise the remediation strategy (DNV GL 2015a). In the corrosion module, a long-term evolution rule for different types of corrosion (i.e., uniform and pitting corrosion) associated with the probability distributions of the corrosion characteristics, e.g., pit depth and shape, are provided (Melchers 2021; Shekari et al. 2017). As shown in Fig. 2.a, based on the output of the corrosion module, one can determine the severity of the corrosion in terms of corrosion Intensity Measure (IM) for a given time of exposure (t_1). The IM parameter must be defined based on the dominant corrosion parameters that affect the failure of the components. Additionally, the probability distributions of the corrosion parameters are provided for this specific time of exposure (t_1). Based on these probability distributions for an assumed level of corrosion intensity measure ($IM = im_1$), various pitting morphologies can be considered. Consequently, the variation of pitting morphology can affect the Engineering Demand Parameter (EDP) in which the component fails. EDP is a structural response quantity that can be used to estimate the failure or damage state of a component (Whittaker et al. 2004). In this study, numerical models associated with a micromechanical fracture criterion were analyzed for different stochastic morphologies of pitting corrosion to quantify the probability of failure.

As illustrated schematically in Fig. 2.b, a fragility curve is a cumulative probability distribution function in which the probability of failure for a determined engineering demand parameter (edp_1) can be written as follows:

$$F(edp_1) = P_f(EDP > edp_1 | IM = im_1) \qquad (1)$$

Where $F(edp_1)$ denotes the probability of failure when EDP exceeds edp_1. The right-hand term $P_f(EDP > edp_1 | IM = im_1)$ is calculated from stochastic analyses of the structural component subjected to a set of random pitting morphologies generated for a predefined level of intensity measure ($IM = im_1$). This concept is common practice in earthquake engineering to consider the

uncertainties associated with the frequency content of different ground motions (Deylami and Mahdavipour 2016; Mahdavipour and Deylami 2014).

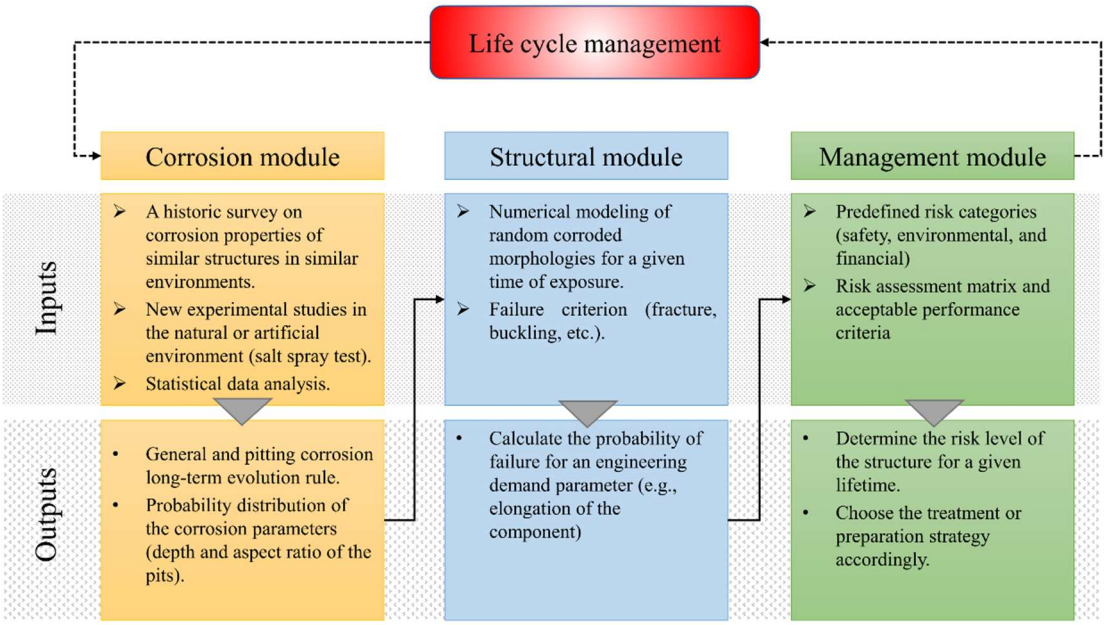

Fig. 1. An overview of the risk-based corrosion management procedure (this study is focused on the structural module).

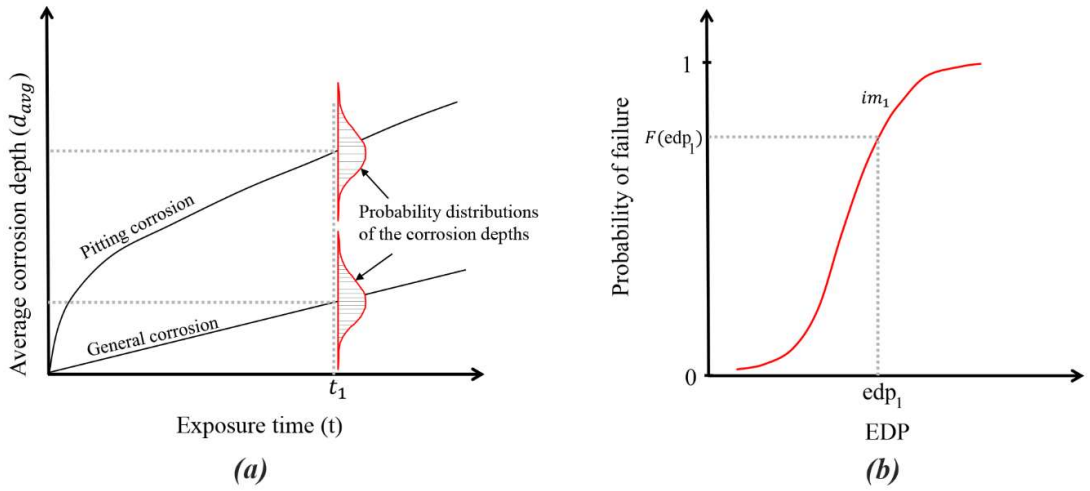

Fig. 2. a) An illustration of the long-term evolution rule and the probability distribution of corrosion parameters, b) an illustration of the concept of fragility curve.

Based on the outputs of the structural modules, decision-makers utilize risk management methods to assess the most critical scenarios in terms of principal criteria, e.g., health and safety, economy, environment, and accordingly prescribe remedies for an expected lifetime (DNV GL 2015a). It is worth mentioning that doing the whole cycle described in Fig. 1 requires a variety of data gathered for a particular project. This study is devoted to making advancements in the structural modules. For this reason, the output of the corrosion module was determined from

relevant literature. Then the fragility curves were developed to scrutinize the effect of involved parameters on the failure probability of components.

2.1.Intensity measure of corrosion

An Intensity Measure (IM) definition is required to describe the severity of future corrosion and involve all influential parameters in the assessment process. For uniform corrosion, the main parameter that can specify the intensity of corrosion is the average corrosion depth, while in pitting corrosion, using one parameter cannot accurately describe the intensity level of the corrosion. One of the conventional IMs is Degree of Pitting (DOP) that provides information about the surficial intensity of pits by calculating the ratio of the corroded area (A_c) to the total area of the original member (A_t) (Huang et al. 2010; Wang et al. 2020; Wang et al. 2014) as follows:

$$DOP(\%) = \frac{A_c}{A_t} \times 100\% \qquad (2)$$

DOP is silent about the pitting depth; however, pit depth was indicated as an influential parameter on the ductility of the tensile components (Sheng and Xia 2017; Xu et al. 2016). Therefore, in this study, an integrated $IM[DOP,\ d_{avg}]$ was used that consists of both Degree of Pitting (DOP) and average pitting depth (d_{avg}). This definition is also consistent with standard methods (ASTM 2005; International Organization for Standardization 2020) proposed for the rating of pitting corrosion.

2.2.Engineering demand parameter

The selection of a proper EDP depends on the nature of the load and the probable failure mode of the component. For example, when the fracture of a tensile member is under investigation, axial elongation of the component can be considered as EDP; however, it must be selected appropriately for other types of components, e.g., steel joints under bending or a compression member. In these components, joint rotation and compressive load can be considered as describing structural responses related to the component failure or damage state.

2.3.Pitting characteristics

Previous studies (Duddu 2014; Xu et al. 2016) showed that when corrosion pits are significantly developed into the thickness of members, the pits can be simplified by semi-ellipsoids. By this simplification, the effect of the pit geometry

can be implemented in finite element models as were done by many other authors (Cerit 2013; Cerit et al. 2009; Huang et al. 2010; Wang et al. 2018a; Yan et al. 2019; Zhang et al. 2015; Zhao et al. 2020).

In this study, a semi-ellipsoidal shape was also assumed as an acceptable geometry to implement pits in the finite element models. Based on this geometry, to characterize a pit, one needs to specify its coordinates (x and y), depth (d), and aspect ratio (AR). AR is defined as the ratio between the pit width (w) and the pit depth ($AR=w/d$) that affects local responses in the pit, i.e., plastic strain and stress triaxiality (Cerit 2013; Cerit et al. 2009; Wang et al. 2018a). These parameters illustrated in Fig.4 can randomly be generated based on the probability distributions of the pit characteristics. Fig. 3 describes the procedure to generate a random pattern based on an assumed time of exposure (t_1) that intensity of the corrosion is $IM[DOP_{(t_1)}, d_{avg(t_1)}]$.

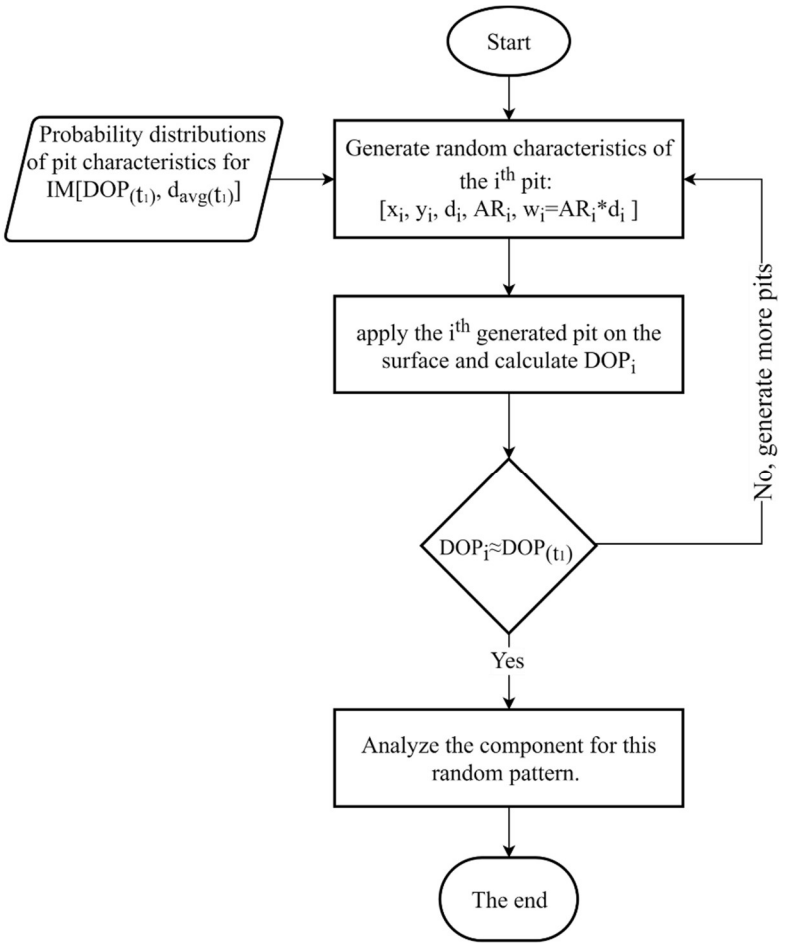

Fig 3. The procedure of random pitting pattern generation for $IM[DOP_{(t_1)}, d_{avg(t_1)}]$.

2.4.Numerical modeling of the random pitting

To evaluate the failure of a component under externally applied load, the finite element model of the component must be analyzed for each generated random

pattern. In this study, a carving technique was proposed to implement different pitting patterns into the numerical models. More details about this technique and also material modeling are presented in the following sections.

2.4.1. Pitting pattern discretization

The meshing technique and proper type of elements to implement corrosion pits depend on the nature of the problem. Previous studies indicated that for steel members under compression where the main failure is a global or local buckling, shell elements are adequate (Wang et al. 2018b; Wang et al. 2014; Zhao et al. 2018; Zhao et al. 2021). The effect of random pitting morphologies can be implemented by changing the thickness of the shell element in the location of the pits (Wang et al. 2018b; Wang et al. 2014; Zhao et al. 2018; Zhao et al. 2021). Alternatively, when the component is under tensile load and fracture is the most dominant failure mode, using solid elements with fine mesh is required to predict the fracture initiation. In contrast to shell elements, solid elements can properly capture the effect of triaxiality and interaction between pits.

On the other hand, for solid elements, implementing a random pattern of semi-ellipsoidal pits in the geometry of components is a demanding task. When the geometry is complicated, and hexahedral elements are employed, the standard meshing techniques provided by numerical software solutions often need manual partitioning and seeding to have a proper mesh quality. The manual meshing techniques are inefficient in implementing a random pitting morphology with lots of different random pits. In most cases, these meshing techniques can lead to divergence or a low-quality mesh. This can be more problematic in this study in which multiple random patterns are under investigation. One possibility is to use tetrahedral elements that support fully automatic tetrahedral meshers (Dassault Systèmes 2014). But for the same degree of freedom and amount of discretization through the thickness of a member, one needs significantly more tetrahedral elements compared to hexahedrons (Wang et al. 2017).

Moreover, the first-order tetrahedral elements are insufficiently accurate for structural calculations (Dassault Systèmes 2014), and the second-order formulation must be chosen that even needs more computational resources. In contrast, developed reduced integration hexahedral elements can significantly increase computational efficiency without losing accuracy (Dassault Systèmes 2014). Therefore, various techniques were employed to implement random pitting corrosion with hexahedral elements (Ahmmad and Sumi 2010; Wang et al. 2014;

Wang et al. 2017). These techniques are mainly developed based on third-party software or code that might be unavailable to the community. In this study, the pits were implemented on the component's geometry by carving the pits on an intact mesh. The geometry of the intact component was discretized with eight-node brick elements with reduced integration (C3D8R). Then the pits were implemented by removing nodes and associated elements located inside the pits. Fig. 4 illustrates this approach to implement the geometry of a single pit on a steel plate.

For micromechanical modeling of ductile fracture, a fine mesh size comparable with the characteristic length (ℓ^*) of the mild steel is required to calculate the local response and the fractured state accurately (Kanvinde and Deierlein 2006; Liao et al. 2012). The characteristic length is defined as a length scale that ductile crack is assumed to initiate once the fracture criteria exceed the critical value over that length (Kanvinde and Deierlein 2006). This mesh refinement must be used over the most critical region of the component due to the unknown locus of fracture initiation. By using such fine mesh, a stepwise representation of pits created by carving on the intact mesh can predict relatively similar local results compared to pits implemented by geometry. This can be tested through a standard mesh sensitivity analysis for a single pit penetrated into the component.

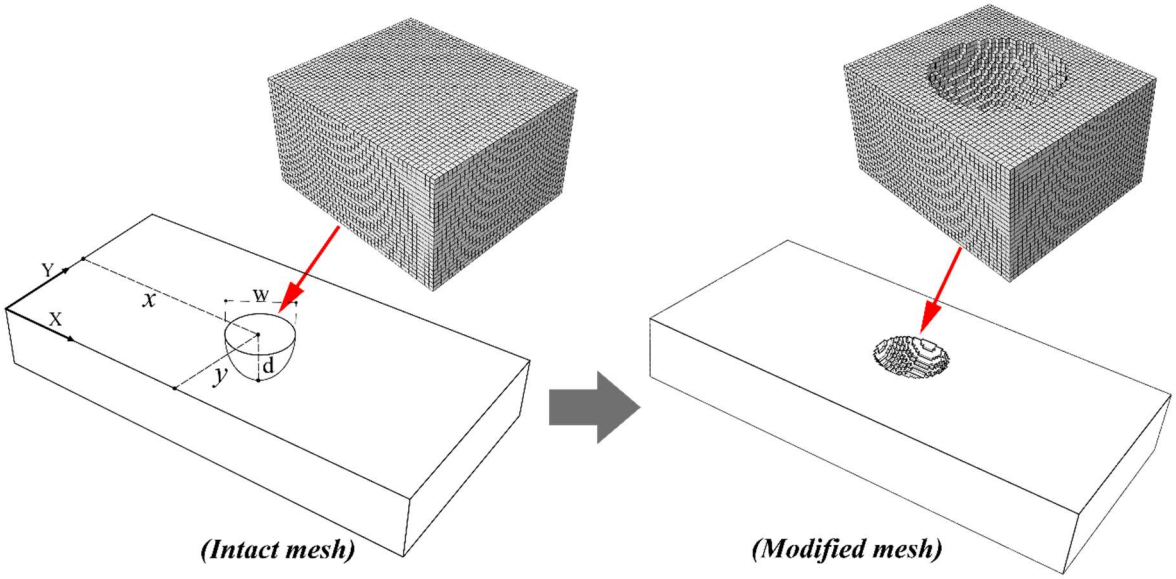

Fig. 4. The geometry of a random pit is implemented by carving on the intact mesh.

2.4.2. Material modeling

The Void Growth Model (VGM) was selected as a micromechanical ductile fracture criterion in which an explicit continuous integration of the stress triaxiality ratio (η) with respect to equivalent plastic strain ($\bar{\varepsilon}_p$) is performed (Kanvinde and Deierlein 2006). Based on the VGM, the fracture initiates when the size of voids

exceeds a threshold value (Kanvinde and Deierlein 2006). Therefore, the criterion can be formulated as follows (Kanvinde 2017):

$$VGI = \int_0^{\bar{\varepsilon}_p} e^{1.5\eta} . d\bar{\varepsilon}_p > VGI_{critical} \qquad (3)$$

The left-hand side of this relation is the Void Growth Index (*VGI*) that is calculated by an explicit integration of stress triaxiality ratio (η) with respect to equivalent plastic strain history ($\bar{\varepsilon}_p$) (Kanvinde and Deierlein 2006; Kanvinde and Deierlein 2007). The critical void growth index ($VGI_{critical}$) on the right-hand side can be considered as a material parameter that is calibrated based on the smooth-notched tensile specimens and complementary finite element analyses (Kanvinde and Deierlein 2006; Kanvinde and Deierlein 2007).

Besides the fracture criterion, an element removal technique was used to model the fracture propagation through the components that remove elements with *VGI* larger than $VGI_{critical}$. It was indicated that the VGM can effectively be used to simulate material separation through finite element removal techniques (Saykin et al. 2020).

3. A Case study

To present a demonstration of the described method, fracture-based fragility curves were extracted for a simple pulling dogbone specimen under different intensity levels of pitting corrosion. This plate can be considered as a local representative of an actual steel component.

3.1.Specimen geometry

Fig. 5 shows the geometry of the intact specimen. It was assumed that only the uniform reduced length (30x50mm) is under corrosion attack. The corrosion outside of this region is not critical due to the larger cross-sectional area. The plate was taken from an IPE 200 steel beam flange and machined into a 7.4 mm thickness (Mahdavipour and Vysochinskiy 2021).

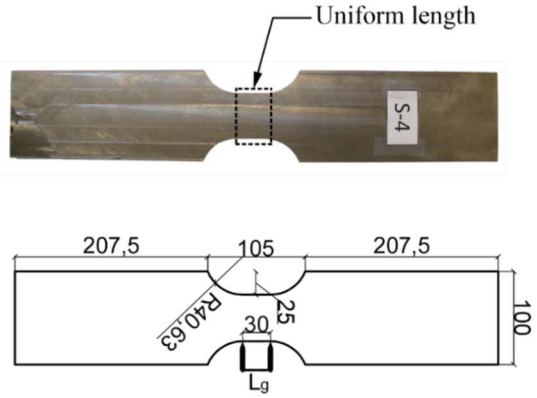

Fig. 5. The geometry of the intact tensile plate from S355J2 steel material (all dimensions are in mm and the thickness of the plate is 7.4mm) (Mahdavipour and Vysochinskiy 2021).

3.2.Specimen material

The specimen was fabricated from European steel grade S355J2 (European Committee for Standardization 2004). Fig. 6.a presents the plastic flow curve of S355J2 calibrated by Mahdavipour and Vysochinskiy (2021). This flow curve was employed with von Mises yield criterion and associated isotropic hardening to simulate material plasticity (Mahdavipour and Vysochinskiy 2021). The calibration of the VGM for S355J2 steel based on notched specimens also showed an average of 3.09 for $VGI_{critical}$ (Mahdavipour and Vysochinskiy 2021). In terms of elastic properties, Young's modulus (E) and Poisson's ratio (v) were assumed to be 191 GPa and 0.3, respectively. Fig. 6.b compares the numerical and experimental force-elongation of the intact specimen. This figure indicates a good agreement between numerical and experimental results. More validation tests also can be found in (Mahdavipour and Vysochinskiy 2021).

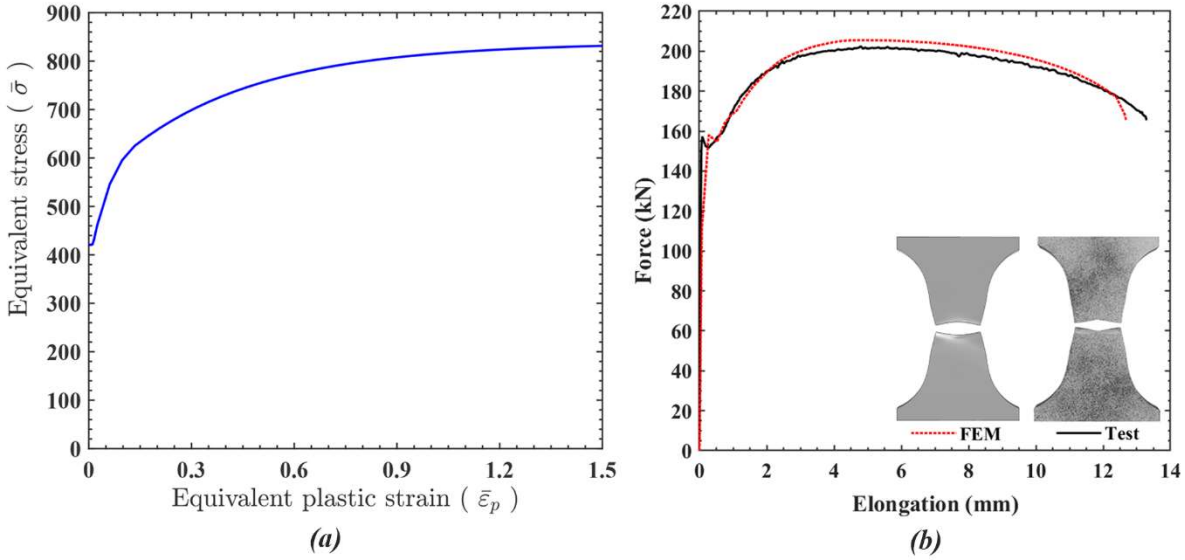

Fig. 6. a) Plastic flow curve of S355J2 used in numerical models (Mahdavipour and Vysochinskiy 2021), b) A comparison between numerical curve obtained in this study and experimental curve reported by (Mahdavipour and Vysochinskiy 2021).

3.3.Numerical modeling of specimen

Abaqus finite element software based on an explicit integration scheme was used to model intact and corroded specimens. A VUSDFLD user subroutine was developed to employ VGM as a fracture criterion in the numerical models.

Since guidelines like DNVGL-CG-0172 and DNVGL-CG-0182 (DNV GL 2015b; DNV GL 2016) define 60%-70% of the original plate thickness as a minimum acceptable remaining thickness without repair, 3 mm was considered as the maximum pit depth when pitting intensities were defined. In other words, repairing is necessary when pits are penetrated more than 3 mm in the studied plate. Based on this limitation, a standard mesh sensitivity analysis for a single pit with a 3 mm depth penetrated at the center of the plate was carried out. The pit was implemented by carving on the intact mesh with different sizes (0.7-0.3 mm) also by direct implementation of the geometry of the pit. Fig. 7 compares the *VGI* distribution in the pit for different mesh sizes.

The results indicate that by decreasing the mesh size from 0.4 mm to 0.3 mm, the maximum *VGI* changed less than 1%. This slight variation implies that mesh size is converged, and using 0.4 mm mesh size is adequate to evaluate local response in the pit domain. On the other hand, the element size must also be comparable with the typical characteristic length (ℓ^*) of mild steels that is reported from 0.4 mm to 0.2 mm (Kanvinde and Deierlein 2006; Liao et al. 2012). Based on these two factors, a 0.3 mm mesh size was selected for the discretization of the uniform length of the specimen; however, this element size must be reverified if thicker plates with deeper pits are under investigation.

As Fig.7 indicates, the maximum *VGI* obtained from carving on 0.3 mm mesh size showed less than 7% difference with the pit implemented by geometry. It must be remembered that using ideal smooth semi-ellipsoidal pits in itself is a simplification of the overall geometry of pits; however, the natural pits can have irregular surfaces. Therefore, this difference should not be interpreted as an absolute error but indicate that carving pits can predict the local effect of pit reasonably. It is also worth mentioning that although the carved pit could capture the maximum *VGI* observed in the pit, the *VGI* distribution fluctuates due to the stepwise nature of the carving approach (see Fig. 4). Since the maximum *VGI* controls the fracture initiation, the form of distribution is less influential on the final pit fracture behavior. Fig. 8 shows the final mesh configuration of the intact specimen as well as presents an example of a carved mesh for a random pitting pattern.

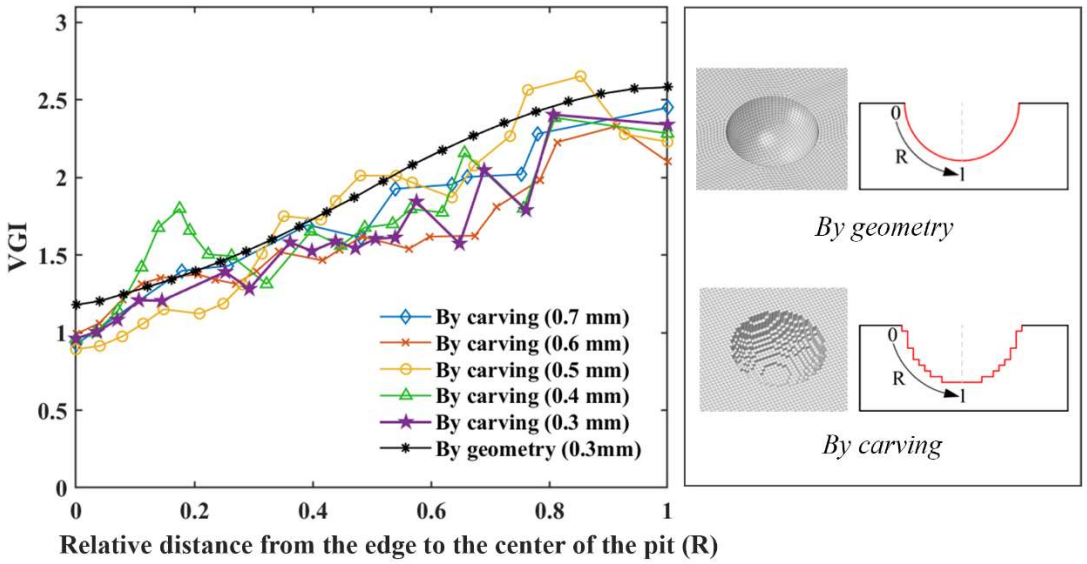

Fig. 7. Sensitivity of the VGI to the mesh size for a single pit carved at the center of the plate.

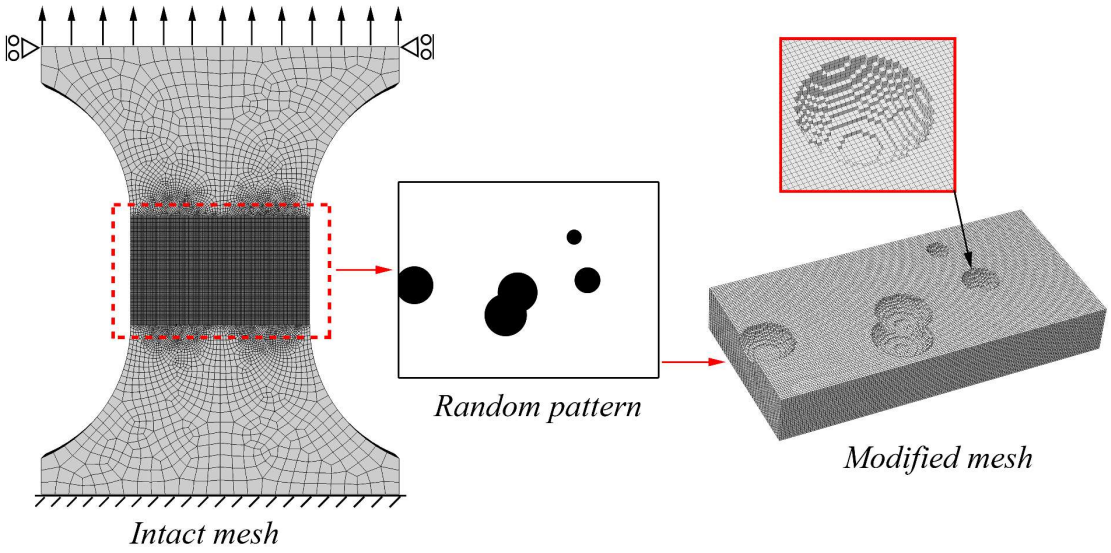

Fig. 8. An illustration of the implementation of a random pitting pattern by carving on the intact mesh.

3.4.Selected pitting IMs

Based on IM definition, nine different levels of IM were considered as listed in Table 1. Fifty random pitting morphologies were generated for each level based on the probability distribution of the pitting characteristics. The number of realizations discussed later by statistical analyses of the simulation results. It must be noted these predefined levels of intensity were selected only to extend the methodology into an application based on *DOPs* smaller than 50%. This limitation was adapted from reputable guidelines (DNV GL 2015; DNV GL 2016) that consider *DOPs* greater than 50% as uniform corrosion. As mentioned before, in an actual project, the target level of pitting corrosion is defined and updated

through a life cycle assessment based on the corrosion evolution rules, periodic inspections, and an expected lifespan, as described in Fig. 1.

Table 1. Matrix of predefined levels of intensity measure of pitting corrosion, $IM[DOP, d_{avg}]$.

		d_{avg}		
		1 mm	2 mm	3 mm
DOP	5%	*IM[5%, 1mm]*	*IM[5%, 2mm]*	*IM[5%, 3mm]*
	10%	*IM[10%, 1mm]*	*IM[10%, 2mm]*	*IM[10%, 3mm]*
	30%	*IM[30%, 1mm]*	*IM[30%, 2mm]*	*IM[30%, 3mm]*

3.5.Selected EDP

Since the specimen is under tensile load and the fracture is the failure mode, the elongation in the uniform length was considered as EDP. Fig. 5 shows the 30 mm of gage length that the elongation was measured for the intact and corroded plates. Based on this parameter, the failure elongation was determined as an elongation in which the strength of the plate dropped sharply. It is important to realize that for other types of components, e.g., connections, finding an obvious point that shows failure is difficult due to structural redundancy and alternative paths to transfer the applied load to other parts. In such cases, a certain amount of strength reduction can be recognized as the failure point.

3.6.Distribution of the pit characteristics

As described in Fig. 3, random pit generation was executed based on the probability distributions of the pit characteristics. These distributions were obtained based on a literature survey on pitting corrosion in mild steel. The position vector (x, y) of each pit center was generated based on uniform distribution (Xia et al. 2021). In this connection, overlapping of the pits was also allowed to consider the intersection of pits and create a larger area of wall thinning. Statistical analyses on naturally and artificially corroded structures showed that the pit depth and aspect ratio follow lognormal distribution (Wang et al. 2018b; Xia et al. 2021). The average pit depth is a time-dependent parameter estimated for a specific environment and expected exposure time. As noted in Table 1, three different average pit depths were assumed (d_{avg} =1mm, 2mm, 3mm). The logarithmic standard deviation of the depth of the pits ($\sigma_{\ln(d)}$) was observed from 0.1 to 0.5 without an obvious trend of change during the time of exposure (Xia et al. 2021). Therefore, a 0.3 constant logarithmic standard deviation of pit depth was considered for all average pit depths in this study. The *AR* is also time-dependent

so that during the time of exposure, the pits change from shallow-wide pits (AR=60) into deep-narrow pits (AR=5) (Xia et al. 2021). Since well-penetrated pits are the most influential pits on ductile fracture (Wang et al. 2018a; Xu et al. 2016), a 5:1 width to depth ratio was assumed as the average aspect ratio (AR_{avg}) with a 0.6 logarithmic standard deviation ($\sigma_{\ln(AR)}$) (Xia et al. 2021). It is worth mentioning that the logarithmic standard deviation of AR was also reported unchanged during the exposure time (Xia et al. 2021). It is also important to realize that although the selected averages and standard deviations do not imply a specific real situation, they are reasonable values adopted to expand the methodology into an application. All these distributions are summarized as follows:

$$\begin{cases} x = Uniform\,[x_1 \;\; x_2] \\ y = Uniform\,[y_1 \;\; y_2] \\ d = Lognormal\left(d_{avg}, \sigma_{\ln(d)}\right) \;\; where \quad d_{avg} = 1mm, 2mm, 3mm\,;\; \sigma_{\ln(d)} = 0.3 \\ AR = Lognormal\left(AR_{avg}, \sigma_{\ln(AR)}\right) \;\; where \quad AR_{avg} = 5{:}1\,;\; \sigma_{\ln(AR)} = 0.6 \\ w = d \times AR \end{cases} \qquad (4)$$

Where x_1, x_2, y_1 and y_2 specify the plate boundaries.

4. Results and discussion

For each nine intensity measures listed in Table 1, the intact mesh of the specimen was modified and analyzed for fifty randomly generated pitting morphologies. Fig 9 shows the force-elongation curves for IM[5%, 2mm], IM[10%, 2mm] and IM[30%, 2mm]. The ultimate and failure points of each curve are highlighted in this figure. In addition, the failure elongation of the intact specimen is also provided for better comparison.

The distribution of the highlighted points indicates that different random pitting morphologies with an identical intensity measure could change the capacity and deformability of the specimen. Statistical parameters for ultimate load and failure elongation are listed in Table 2.

4.1.Effect of random pitting on the ultimate load

Based on the obtained coefficients of variation, the ultimate load of the specimen experienced less than 6.5% of dispersion. Low dispersion indicates that details of pitting corrosion have a negligible effect on the ultimate load variation. As a result, a simplified method without pitting details can be employed to predict the ultimate load. The average reduction in ultimate load is 23.5% in the worst case (i.e.,

IM[30%,3mm]). Fig. 10 also indicates that the decrease in the ultimate capacity of the specimen is correlated with both d_{avg} and *DOP* by -0.52 and -0.72 correlation coefficients, respectively. These coefficients imply a meaningful correlation between these parameters.

4.2. Effect of random pitting on the failure elongation

According to Table 2, the failure elongation exhibited 12.6%-30.2% of dispersion due to variation of pitting pattern. This dispersion demonstrates the effect of pitting details on the ductility of the specimen by triggering the fracture initiation and propagation in different modes. Fig. 12 illustrates the most dominant modes that pitting affected fracture initiation and propagation. As shown in this figure, the fracture initiated at the centroid of the cross-section of the intact specimen and propagated towards the edges. Based on these results, the most critical section with the highest *VGI* demand is the center of the intact specimen. In some patterns, the fracture initiation was triggered by the occurrence of pits (not necessarily deep pits) at this critical location. In some other patterns, a deep pit was generated based on the described probability distributions for pit characteristics (refer to Eq. 4). This deep pit produced higher triaxiality and reduced the fracture strain so that an accelerated fracture initiated at the root of the pit and propagated through the plate. In addition, as Fig. 12 illustrates, the interaction between neighboring pits and interaction between pits and the edge of the plate could also expedite the fracture initiation. In some realizations, a combination of these modes was observed. These results indicate, if a simplified method rather than solid modeling is used, that method must address all these possible effects of pitting appropriately.

Fig. 11 indicates that the reduction in deformability of specimen is correlated with both d_{avg} and *DOP* by -0.75 and -0.33 correlation coefficients, respectively. Therefore, deeper and denser pitting patterns led to more reduction in failure elongation; however, the effect of d_{avg} was more significant. This correlation also highlights the use of the integrated IM that identifies the level of the pitting corrosion based on both degree of pitting (*DOP*) and pit average depth (d_{avg}). According to Table 2, for the greatest intensity measure, i.e., IM[30%,3mm], the elongation reduced by 66% on average compared to the intact specimen. This reduction rate is an extreme deterioration in terms of deformability.

Table 2. Statistical parameters of the ultimate load and failure elongation.

	Ultimate load				Failure elongation			
Pitting intensity	Average (kN)	Standard deviation (kN)	Coefficient of variation (%)	Average reduction of the ultimate load (%)	Average (mm)	Standard deviation (mm)	Coefficient of variation (%)	Average reduction of the failure elongation (%)
IM[5%,1mm]	202.5	0.76	0.37	1.4	10.7	1.52	14.2	13.6
IM[5%,2mm]	199.2	2.32	1.16	3.1	8.1	1.65	20.4	34.6
IM[5%,3mm]	194.6	4.11	2.11	5.3	6.1	1.45	23.8	50.7
IM[10%,1mm]	199.8	1.06	0.53	2.76	9.8	1.34	13.7	20.8
IM[10%,2mm]	193.5	3.18	1.64	5.85	7.1	1.5	21.1	42.6
IM[10%,3mm]	185.9	6.32	3.40	9.55	5.3	1.42	26.8	57.2
IM[30%,1mm]	190.3	2.01	1.06	7.39	8.8	1.11	12.6	28.9
IM[30%,2mm]	174.9	6.72	3.84	14.9	5.8	1.34	23.1	53.2
IM[30%,3mm]	157.1	10.06	6.41	23.5	4.2	1.27	30.2	66.1

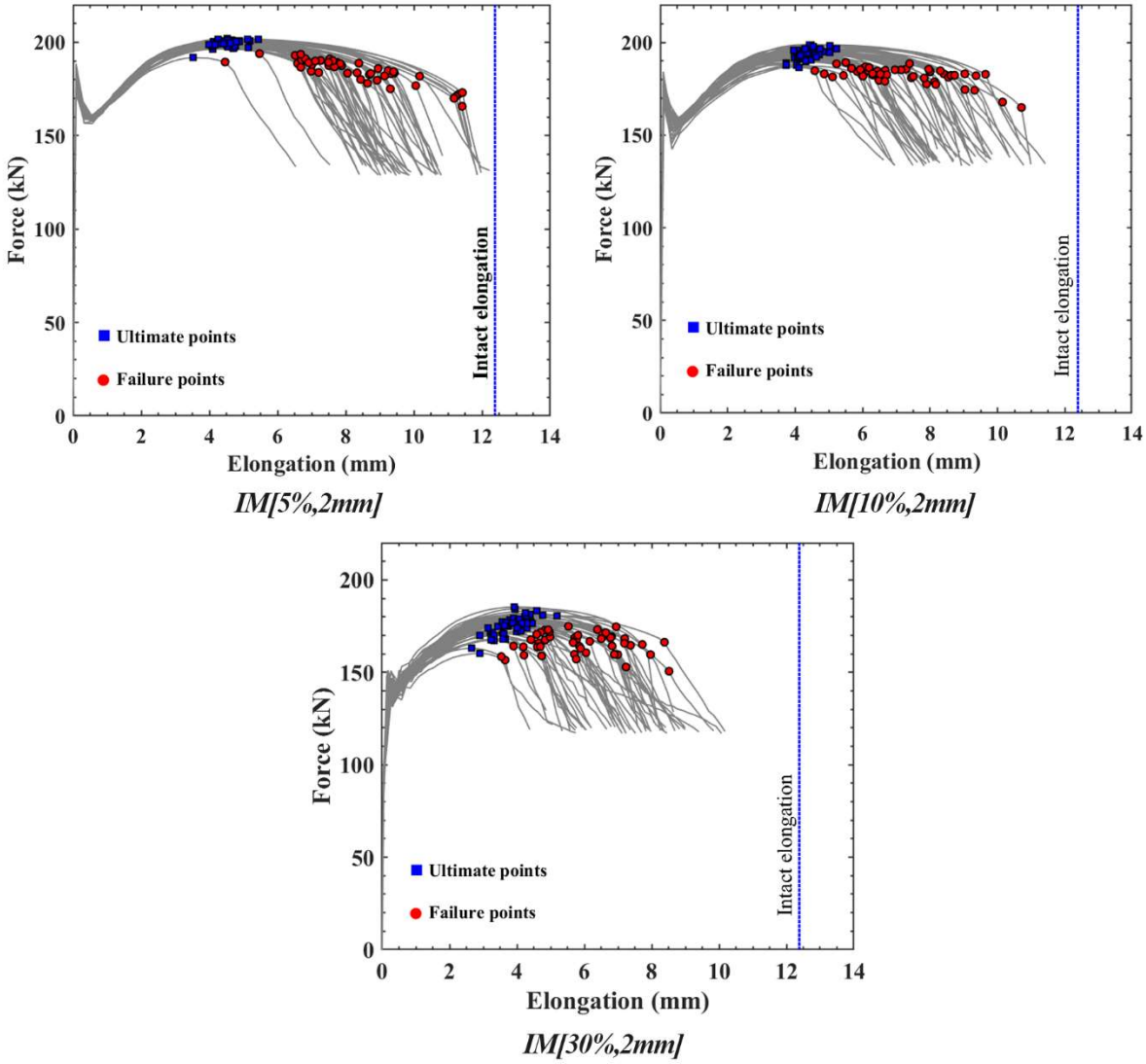

Fig. 9. Force-elongation curves for 2 mm average pit depth and different DOPs.

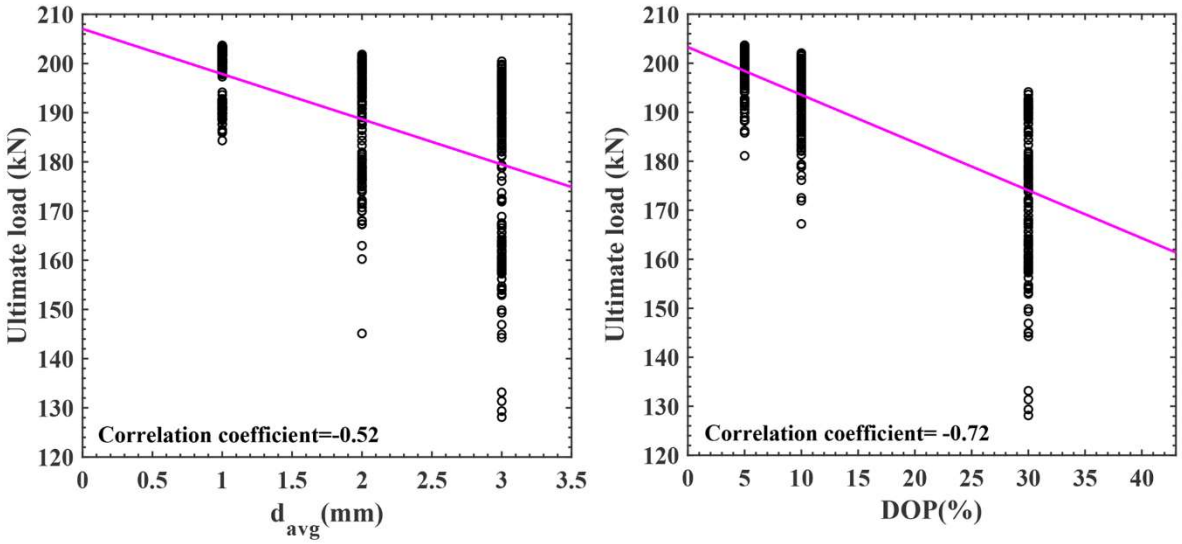

Fig. 10. The ultimate load is correlated with DOP and d_{avg}.

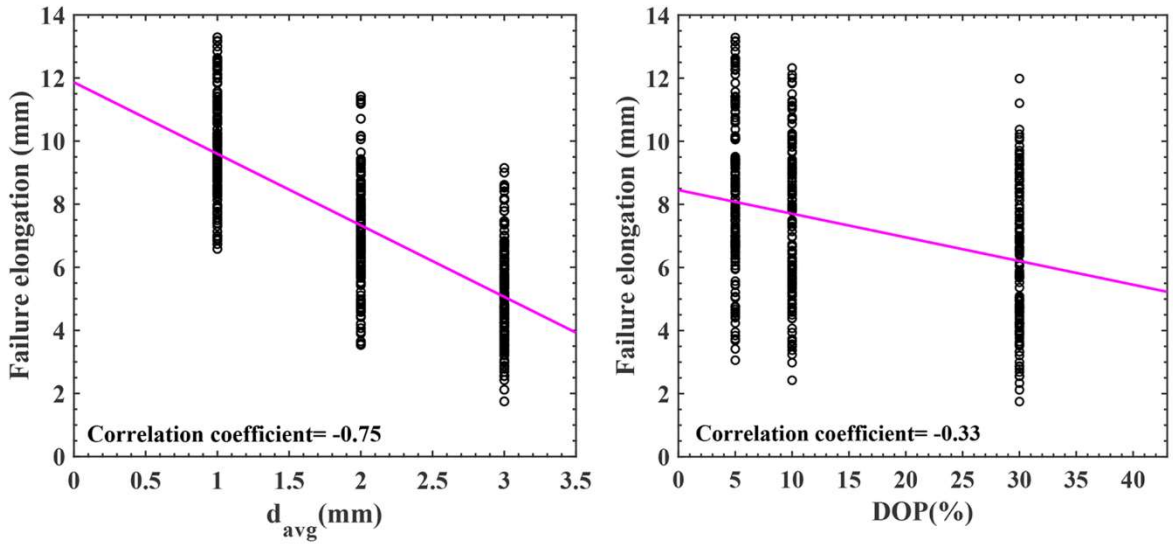

Fig. 11. The failure elongation is correlated with DOP and d_{avg}.

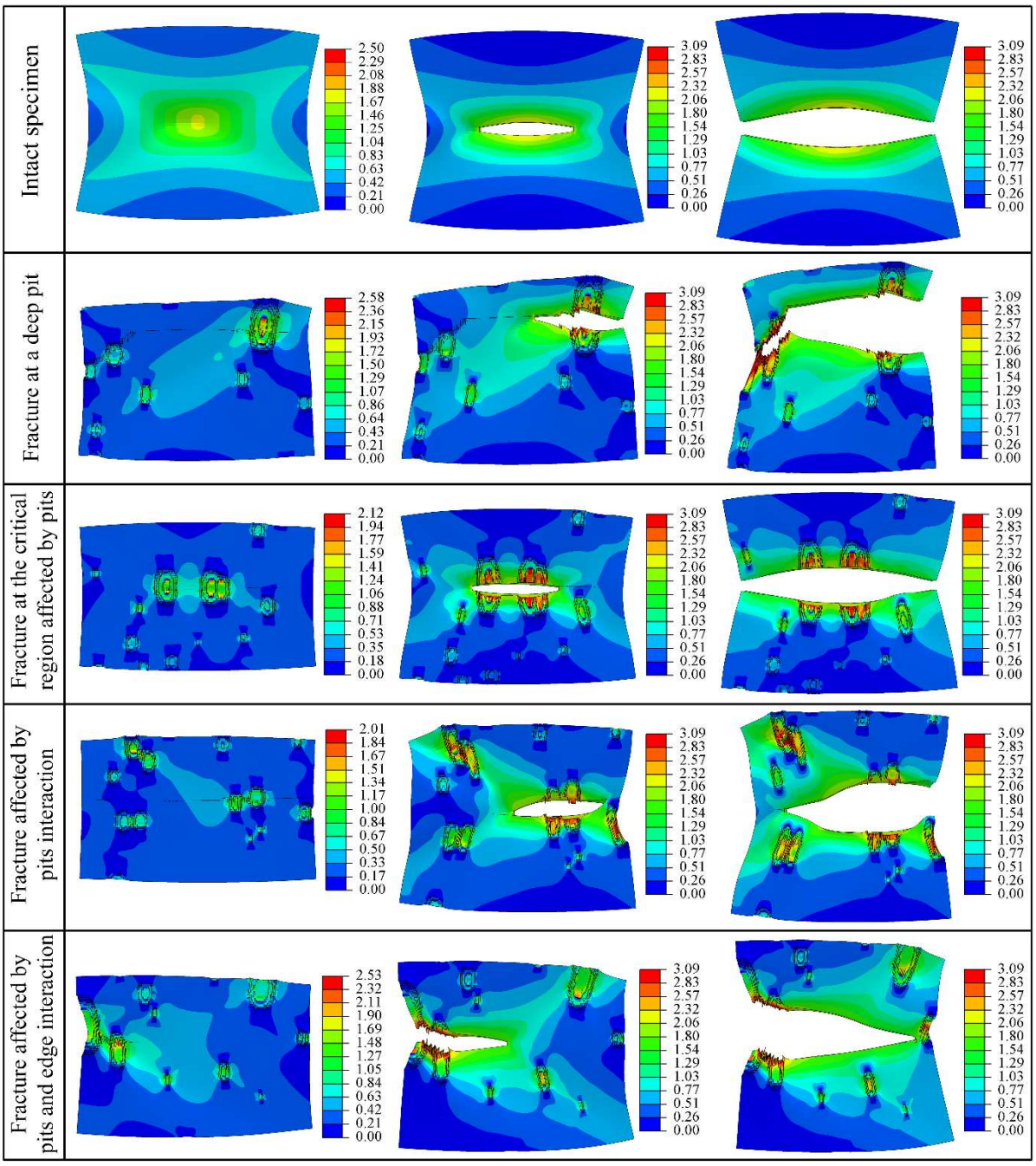

Fig. 12. Different modes of fracture initiation were observed under the effect of pitting corrosion. Contours show the VGI distribution.

4.3.Component fragility curves

Empirical Cumulative Distribution Function (ECDF) was calculated based on the fifty failure elongations for each intensity measure. These fragility curves provide the probability of failure for a given elongation as described in Eq. 1. Fig. 13 shows these fragility curves for a given *DOP* and different d_{avg} (1 mm, 2 mm, and 3 mm). Large Differences between these curves denote the significant effect of pitting characteristics on the deformability of the specimen. It is worth mentioning that

for using these curves, the demand elongation of the component must be estimated based on the analysis of the global structure. It must also be reminded that for a specific environment and exposure time, only one fragility curve is required to use in the risk-based corrosion management procedure as described in Fig. 1.

To compare these ECDFs with Lognormal, Normal, and Weibull (two-parameter) distributions, two-sample Kolmogorov–Smirnov (K-S) tests at a 5% significance level were used. K-S is a common nonparametric test method to check whether two datasets of samples are describing the same probability distribution or not (Sprent and Smeeton 2016). The goodness of fit was evaluated based on the K-S output parameters (statistic and P-value). These results indicated a better fit for all curves when a Lognormal distribution was used. The fitted Lognormal curves are also presented in Fig. 13.

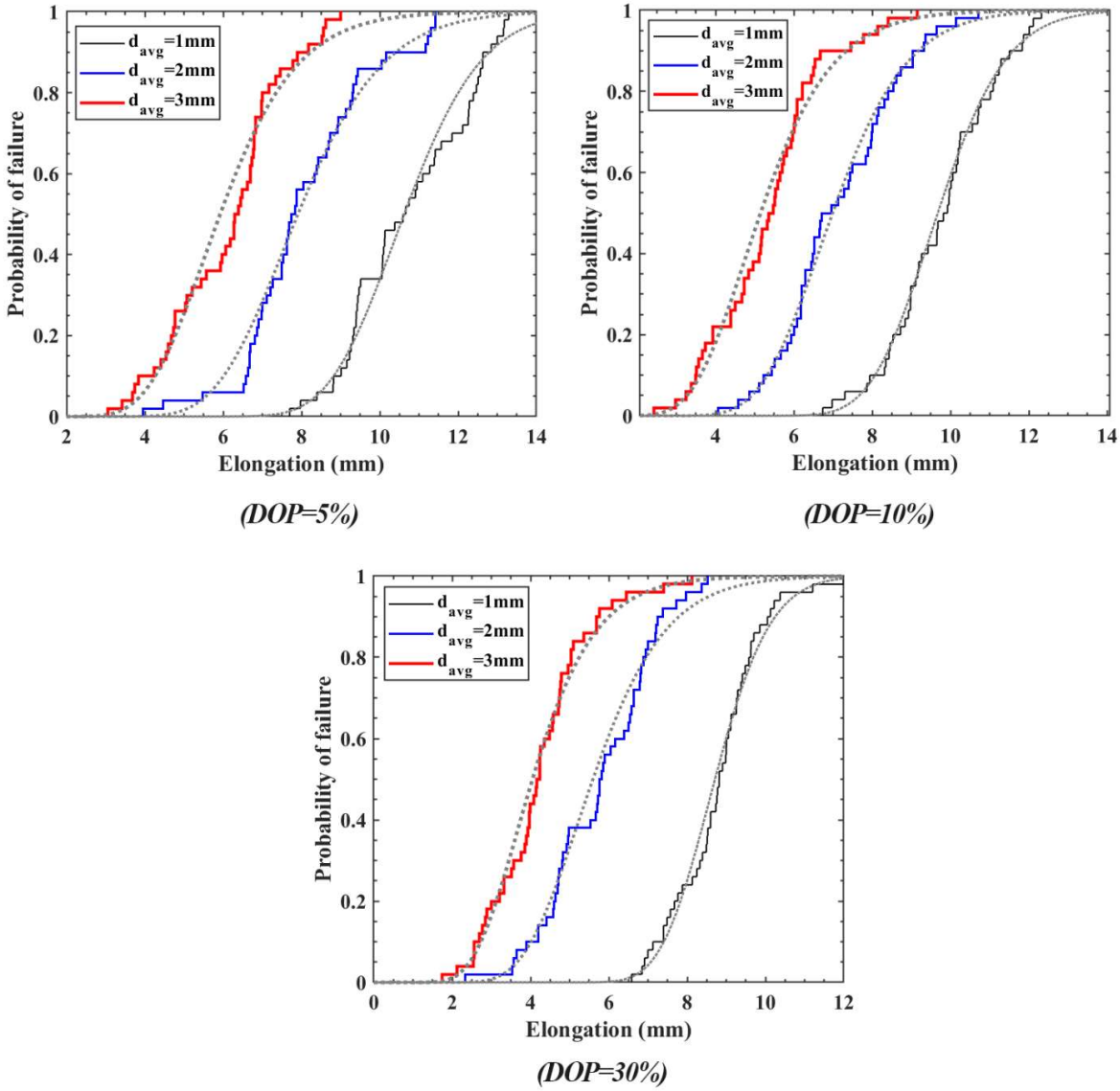

Fig. 13. Fragility curves obtained for various DOP and d_{avg} (dotted curves denote fitted lognormal distributions)

4.4.Number of random morphologies

Using more random morphologies can help enhance the accuracy of the ECDFs of the failure elongation; meanwhile, it can increase the computational time and cost. In this study, fifty random pitting morphologies were initially evaluated; however, the failure elongation resulted from numerical models showed that using fewer patterns also can predict the results with the approximately same distribution. For this reason, the ECDFs of datasets with fewer pitting morphologies (i.e., 5, 10, 20, 30, and 40) were compared to the ECDF from fifty morphologies. The results of the two-sample K-S test at a 5% significance level for all intensity measures indicate that twenty random morphologies can describe the ECDFs as almost accurate as fifty random morphologies.

5. Conclusions

Steel structures can experience excessive plastic deformations during their lifetime due to extreme events. Under a corrosive environment, the interaction of pitting corrosion and plastic deformation can affect the integrity of the steel components because of an accelerated ductile fracture. Therefore, pitting corrosion must be addressed appropriately to evaluate structural capacity and ductility during corrosion risk management procedures.

This study proposed fracture-based fragility curves as tools that provide the probability of failure for a given intensity level of the pitting corrosion. A two-parameter intensity measure was defined to describe the severity of the pitting corrosion based on the degree of pitting and the average depth of pits. For a predefined intensity level, the fragility curves can be obtained by analyzing the failure of steel components for various random pitting patterns generated according to the probability distributions of the pit characteristics (location, depth, aspect ratio). A demonstration study on a tensile plate subjected to single-sided pitting corrosion at different levels of intensity measure showed that the developed fragility curves are powerful tools to consider the morphology-to-morphology uncertainties in structural evaluations.

According to obtained fragility curves, both degrees of pitting (*DOP*) and the average depth of pits are influential on the probability of failure. However, the effect of average depth was more significant. It was observed that for a given intensity level of corrosion, the variation on the failure elongation of the plate could exceed 30%. In comparison, the dispersion in ultimate load was limited to 6.4%. The significant variation of failure elongation was derived from different

modes that corrosion pits triggered fracture initiation in various random morphologies. The interaction of two pits, the interaction between pits and the edge of the plate, and the existence of a well-penetrated pit are the most dominant modes that corrosion pits accelerate the ductile fracture initiation. In contrast, the low variation in ultimate load demonstrated that pitting details is less critical in predicting the ultimate capacity of the components.

In addition, the effect of the number of random morphologies on the fragility curves was investigated by Kolmogorov–Smirnov tests. The results revealed that using twenty random morphologies is adequate to describe the fragility curves of the studied specimen; however, this number can vary by specimen configuration. Therefore, the number of random morphologies for other specimen configurations must be determined based on a similar procedure to capture all possible fracture initiation modes.

The proposed method coupled with corrosion data and risk management procedures can be used for the life cycle evaluation of new or existing steel structures under excessive plastic deformations and corrosive environments. However, the main challenge regarding the applicability of the method is the considerable required computational resources. This is mainly attributable to the fine mesh of solid elements used for ductile fracture prediction. Future studies must move towards an optimal modeling technique in which all described effects of random pits can be involved in the failure of steel components with less computational effort.

6. References

Ahmmad, M. M., and Sumi, Y. (2010). "Strength and deformability of corroded steel plates under quasi-static tensile load." *Journal of marine science and technology*, 15(1), 1-15.

ASTM (2005). "Standard guide for examination and evaluation of pitting corrosion (G46-94)." ASTM International.

Bao, Y., and Wierzbicki, T. (2004). "On fracture locus in the equivalent strain and stress triaxiality space." *International Journal of Mechanical Sciences*, 46(1), 81-98.

Cerit, M. (2013). "Numerical investigation on torsional stress concentration factor at the semi elliptical corrosion pit." *Corrosion Science*, 67, 225-232.

Cerit, M., Genel, K., and Eksi, S. (2009). "Numerical investigation on stress concentration of corrosion pit." *Engineering failure analysis*, 16(7), 2467-2472.

Dassault Systèmes (2014). *ABAQUS Analysis User's Manual (Version 6.14)*, Dassault Systèmes Simulia Corp., Providence, RI.

Deylami, A., and Mahdavipour, M. (2016). "Probabilistic seismic demand assessment of residual drift for Buckling-Restrained Braced Frames as a dual system." *Structural Safety*, 58, 31-39.

DNV GL (2015a). "Risk based corrosion management (DNVGL-RP-C302)." DNV GL AS.
DNV GL (2015b). "Thickness diminution for mobile offshore units (DNVGL-CG-0172)." DNV GL AS.
DNV GL (2016). "Allowable thickness diminution for hull structure (DNVGL-CG-0182)." DNV GL AS.
Duddu, R. (2014). "Numerical modeling of corrosion pit propagation using the combined extended finite element and level set method." *Computational Mechanics*, 54(3), 613-627.
European Committee for Standardization (2004). "Standard for hot-rolled structural steel. Part 2 - Technical delivery conditions for non-alloy structural steels (EN 10025-2:2004).", CEN, Brussels, Belgium.
Ghosh, J., and Padgett, J. E. (2010). "Aging considerations in the development of time-dependent seismic fragility curves." *Journal of Structural Engineering*, 136(12), 1497-1511.
Guo, X., and Zhang, C. (2019). "Seismic fragility analysis of corroded chimney structures." *Journal of Performance of Constructed Facilities*, 33(1), 04018087.
Hancock, J., and Mackenzie, A. (1976). "On the mechanisms of ductile failure in high-strength steels subjected to multi-axial stress-states." *Journal of the Mechanics and Physics of Solids*, 24(2-3), 147-160.
Huang, Y., Zhang, Y., Liu, G., and Zhang, Q. (2010). "Ultimate strength assessment of hull structural plate with pitting corrosion damnification under biaxial compression." *Ocean Engineering*, 37(17-18), 1503-1512.
International Organization for Standardization (2020). "ISO 11463: Corrosion of metals and alloys - Guidelines for the evaluation of pitting corrosion."
Jahanitabar, A. A., and Bargi, K. (2018). "Time-dependent seismic fragility curves for aging jacket-type offshore platforms subjected to earthquake ground motions." *Structure and Infrastructure Engineering*, 14(2), 192-202.
Ji, J., Zhang, C., Kodikara, J., and Yang, S.-Q. (2015). "Prediction of stress concentration factor of corrosion pits on buried pipes by least squares support vector machine." *Engineering Failure Analysis*, 55, 131-138.
Johnson, G. R., and Cook, W. H. (1985). "Fracture characteristics of three metals subjected to various strains, strain rates, temperatures and pressures." *Engineering fracture mechanics*, 21(1), 31-48.
Kanvinde, A. (2017). "Predicting fracture in civil engineering steel structures: State of the art." *Journal of Structural Engineering*, 143(3), 03116001.
Kanvinde, A., and Deierlein, G. (2006). "The void growth model and the stress modified critical strain model to predict ductile fracture in structural steels." *Journal of Structural Engineering*, 132(12), 1907-1918.
Kanvinde, A., and Deierlein, G. (2007). "Finite-element simulation of ductile fracture in reduced section pull-plates using micromechanics-based fracture models." *Journal of Structural Engineering*, 133(5), 656-664.
Lemaire, M. (2013). *Structural reliability*, John Wiley & Sons.
Liao, F., Wang, W., and Chen, Y. (2012). "Parameter calibrations and application of micromechanical fracture models of structural steels." *Structural engineering and mechanics*, 42(2), 153-174.
Mahdavipour, M., and Deylami, A. (2014). "Probabilistic assessment of strain hardening ratio effect on residual deformation demands of Buckling-Restrained Braced Frames." *Engineering structures*, 81, 302-308.

Mahdavipour, M. A., and Vysochinskiy, D. (2021). "Using a DIC-based approach to enhance the calibration accuracy of the void growth model ductile fracture criterion." Unpublished manuscript,University of Agder

McClintock, F. A. (1968). "A criterion for ductile fracture by the growth of holes." *Journal of applied mechanics*, 35(2), 363-371.

Melchers, R. E. (2021). "New insights from probabilistic modelling of corrosion in structural reliability analysis." *Structural Safety*, 88, 102034.

Pidaparti, R. M., and Patel, R. R. (2008). "Correlation between corrosion pits and stresses in Al alloys." *Materials Letters*, 62(30), 4497-4499.

Rice, J. R., and Tracey, D. M. (1969). "On the ductile enlargement of voids in triaxial stress fields." *Journal of the Mechanics and Physics of Solids*, 17(3), 201-217.

Saykin, V. V., Nguyen, T. H., Hajjar, J. F., Deniz, D., and Song, J. (2020). "The effect of triaxiality on finite element deletion strategies for simulating collapse of full-scale steel structures." *Engineering Structures*, 210, 110364.

Shekari, E., Khan, F., and Ahmed, S. (2017). "Probabilistic modeling of pitting corrosion in insulated components operating in offshore facilities." *ASCE-ASME J Risk and Uncert in Engrg Sys Part B Mech Engrg*, 3(1).

Sheng, J., and Xia, J. (2017). "Effect of simulated pitting corrosion on the tensile properties of steel." *Construction and Building Materials*, 131, 90-100.

Songbo, R., Ying, G., Chao, K., Song, G., Shanhua, X., and Liqiong, Y. (2021). "Effects of the corrosion pitting parameters on the mechanical properties of corroded steel." *Construction and Building Materials*, 272, 121941.

Sprent, P., and Smeeton, N. C. (2016). *Applied nonparametric statistical methods*, CRC press.

Turnbull, A., Wright, L., and Crocker, L. (2010). "New insight into the pit-to-crack transition from finite element analysis of the stress and strain distribution around a corrosion pit." *Corrosion Science*, 52(4), 1492-1498.

Wang, H., Xu, S., Wang, Y., and Li, A. (2018a). "Effect of pitting degradation on ductile fracture initiation of steel butt-welded joints." *Journal of Constructional Steel Research*, 148, 436-449.

Wang, R., Guo, H., and Shenoi, R. A. (2020). "Compressive strength of tubular members with localized pitting damage considering variation of corrosion features." *Marine Structures*, 73, 102805.

Wang, R., Shenoi, R. A., and Sobey, A. (2018b). "Ultimate strength assessment of plated steel structures with random pitting corrosion damage." *Journal of Constructional Steel Research*, 143, 331-342.

Wang, Y., Wharton, J. A., and Shenoi, R. A. (2014). "Ultimate strength analysis of aged steel-plated structures exposed to marine corrosion damage: A review." *Corrosion Science*, 86, 42-60.

Wang, Y., Xu, S., Wang, H., and Li, A. (2017). "Predicting the residual strength and deformability of corroded steel plate based on the corrosion morphology." *Construction and Building Materials*, 152, 777-793.

Whittaker, A., Deierlein, G., Hooper, J., and Merovich, A. (2004). "Engineering demand parameters for structural framing systems." *Report number: ATC-58-2*, 2.

Xia, M., Wang, Y., and Xu, S. (2021). "Study on surface characteristics and stochastic model of corroded steel in neutral salt spray environment." *Construction and Building Materials*, 272, 121915.

Xu, S., Wang, H., Li, A., Wang, Y., and Su, L. (2016). "Effects of corrosion on surface characterization and mechanical properties of butt-welded joints." *Journal of Constructional Steel Research*, 126, 50-62.

Yan, Y., Shao, B., Zhou, X., Song, S., Zhou, X., and Yan, X. (2019). "A study on the influence of double ellipsoidal pitting corrosion on the collapsing strength of the casing." *Engineering Failure Analysis*, 100, 11-24.

Yang, J., Guo, T., Luo, D., and Liu, Z. (2021). "Multiscale Modeling and Seismic Fragility Analysis of Corroded Precast Concrete Frame." *Journal of Performance of Constructed Facilities*, 35(1), 04020128.

Yang, Y., Wu, Q., He, Z., Jia, Z., and Zhang, X. (2019). "Seismic Collapse Performance of Jacket Offshore Platforms with Time-Variant Zonal Corrosion Model." *Applied Ocean Research*, 84, 268-278.

Yeter, B., Tekgoz, M., Garbatov, Y., and Soares, C. G. (2020). "Fragility analysis of an ageing monopile offshore wind turbine subjected to simultaneous wind and seismic load." *Safety in Extreme Environments*, 1-16.

Zhang, J., Liang, Z., and Han, C. (2015). "Effects of ellipsoidal corrosion defects on failure pressure of corroded pipelines based on finite element analysis." *International Journal of Electrochemical Science*, 10, 5036-5047.

Zhao, Z., Liang, B., Liu, H., and Wu, X. (2018). "Influence of pitting corrosion on the bending capacity of thin-walled circular tubes." *Journal of the Brazilian Society of Mechanical Sciences and Engineering*, 40(11), 1-12.

Zhao, Z., Zhang, H., Xian, L., and Liu, H. (2020). "Tensile strength of Q345 steel with random pitting corrosion based on numerical analysis." *Thin-Walled Structures*, 148, 106579.

Zhao, Z., Zheng, C., Zhang, J., Liang, B., and Zhang, H. (2021). "Influence of random pitting corrosion on moment capacity of thin-walled circular tubes subjected to compression force." *International Journal of Pressure Vessels and Piping*, 189, 104260.